Applied Catalysis B: Environmental 313 (2022) 121463

Contents lists available at ScienceDirect

Applied Catalysis B: Environmental

journal homepage: www.elsevier.com/locate/apcatb

Atomically dispersed lewis acid sites meet poly(ionic liquid)s networks for solvent-free and co-catalyst-free conversion of CO_2 to cyclic carbonates

Huaitao Peng [a,b,1], Qiuju Zhang [b,c,1], Yinming Wang [b,c], Honglin Gao [a,*], Nian Zhang [d], Jing Zhou [e], Linjuan Zhang [e], Qiu Yang [f], Qihao Yang [b,c,**], Zhiyi Lu [b,c,**]

[a] National Center for International Research on Photoelectric and Energy Materials, School of Materials and Energy, Yunnan University, Kunming 650091, PR China
[b] Key Laboratory of Advanced Fuel Cells and Electrolyzers Technology of Zhejiang Province, Ningbo Institute of Materials Technology and Engineering, Chinese Academy of Sciences, Ningbo, Zhejiang 315201, PR China
[c] University of Chinese Academy of Sciences, Beijing 100049, PR China
[d] State Key Laboratory of Functional Materials for Informatics, Shanghai Institute of Microsystem and Information Technology, Chinese Academy of Sciences, Shanghai 200050, PR China
[e] Key Laboratory of Interfacial Physics and Technology, Shanghai Institute of Applied Physics, Chinese Academy of Sciences, Shanghai 201800, PR China
[f] Ningbo New Material Testing and Evaluation Center Co., Ltd, Ningbo New Materials Innovation Center, Ningbo, Zhejiang 315201, PR China

ARTICLE INFO

Keywords:
Atomically-dispersed Lewis acid sites
Poly(ionic liquid)s
Carbon-based catalysts
CO_2 cycloaddition

ABSTRACT

The rational integration of multiple functional units into heterogeneous materials to improve catalytic performance is highly desirable for CO_2 value-added processes. Herein, a catalyst composed of porous carbon matrix with atomically dispersed Lewis acid sites (i.e., AlO_5 motifs) and imidazolium-based poly(ionic liquid)s (denoted as PILs@Al-O-C) was fabricated. Compared with pure Al-O-C or PILs, the optimized PILs@Al-O-C exhibits superior catalytic performance (>90% yield) towards cycloaddition reaction of CO_2 and epoxides in the absence of solvent and co-catalyst. The enhanced activity of PILs@Al-O-C is attributed to the synergistic effect among the uniform N sites (Lewis base sites) and abundant bromide anions (nucleophilic agents) in the PILs network, as well as the atomically dispersed Al sites (Lewis acid sites) in the Al-O-C matrix. This work provides an advanced PILs@Al-O-C catalyst for constructing a neat catalytic system towards CO_2 fixation.

1. Introduction

Chemical fixation of carbon dioxide (CO_2) into high value-added organic products has been considered as a promising methodology to eliminate the excessive emission of CO_2 owing to the anthropogenic activities [1–4]. Up to now, a variety of strategies have been applied to realize the catalytic CO_2 transformation (e.g., N-formylation of amines with CO_2, cycloaddition of epoxide with CO_2, CO_2 hydrogenation) [5–19], among which the coupling of CO_2 and epoxides attracted widespread attention due to its 100% atomic efficiency and the various industrial applications of product (i.e., cyclic carbonate). In this context, a diversity of homogeneous Lewis acid/base catalysts [20–26], including ionic liquids, metal complexes and Schiff bases, etc., have been developed for this reaction, while the inherent difficulties in separation and recycling hinder their practical application. In this regard, heterogeneous catalysts featuring atomically-dispersed active sites can be ideal candidates, which generally exhibit excellent activity or/and selectivity, comparable to their homogeneous counterparts [27–35].

To date, a variety of carbon-based catalysts featuring atomically dispersed metal sites (e.g., Zn, Al, Co, Cu) have been extensively investigated in CO_2 cycloaddition reactions [36–40]. It has been demonstrated that the atomically dispersed metal sites with abundant unoccupied orbitals can be employed as the Lewis acid sites to activate the epoxide (reactant), thereby accelerating the ring-opening step. However, the ring-opening process of epoxides cannot be easily achieved with only Lewis acid sites, which usually requires the assistance of halogen anions (e.g., I^-, Br^-, Cl^-) [41–43]. Indeed, tetrabutyl ammonium

* Corresponding author.
** Corresponding authors at: Key Laboratory of Advanced Fuel Cells and Electrolyzers Technology of Zhejiang Province, Ningbo Institute of Materials Technology and Engineering, Chinese Academy of Sciences, Ningbo, Zhejiang 315201, PR China.
E-mail addresses: hlgao@ynu.edu.cn (H. Gao), yangqihao@nimte.ac.cn (Q. Yang), luzhiyi@nimte.ac.cn (Z. Lu).
[1] These authors contributed equally to this work.

https://doi.org/10.1016/j.apcatb.2022.121463
Received 25 January 2022; Received in revised form 22 April 2022; Accepted 26 April 2022
Available online 29 April 2022

bromide (TBAB) as the homogeneous co-catalyst was widely adopted [44–48], which offers Br^- to attack the carbon atom with less steric hindrance in the epoxide to promote the ring-opening step, but its superior solubility makes it difficult to be isolated from the reaction systems. To overcome this challenge, poly(ionic liquid)s (PILs), a relatively new class of functional polymers with intrinsic halogen anions, can be the alternative candidate [49–52]. Despite the encouraging accomplishments, it remains a challenge to develop an efficient heterogeneous catalyst that combines atomically dispersed Lewis acid sites and PILs network to synergistically promote the CO_2 cycloaddition reaction in the absence of solvent and co-catalysts.

In this work, we have rationally fabricated a carbon-based catalyst featuring atomically dispersed AlO_5 motifs (~3.58 wt%,) and imidazolium-based PILs (~32 wt%) network (denoted as PILs@Al-O-C) based on the pyrolysis of Al-based metal-organic frameworks (Al-MIL-53), and the subsequent in-situ polymerization of ionic liquid monomers (Scheme 1). The optimized PILs@Al-O-C catalyst achieves efficient catalytic CO_2 cycloaddition with epoxides in the absence of solvent and co-catalyst (~91% yield), which is significantly better than that of the corresponding single components (PILs: ~64% yield, Al-O-C: ~3% yield). Both experimental and theoretical analyses reveal that the uniform Lewis base sites (i.e., N sites) and abundant nucleophilic anions (i.e., Br^-) from PILs as well as the atomically dispersed Lewis acid sites (i.e., AlO_5 motifs) synergistically promote the activation of epoxides and subsequent CO_2 cycloaddition reaction. As far as we know, this work represents the first attempt on combination of single-atom catalysis with PILs for efficient chemical fixation of CO_2.

2. Experimental section

2.1. Preparation of the catalysts

2.1.1. Preparation of Al-MIL-53

The synthesis was carried out by the following route developed by Ferey, G. et al. with minor modifications [53]. Typically, a mixture containing $Al(NO_3)_3{\cdot}9H_2O$ (13.0 g), terephthalic acid (2.88 g), de-ionized water (50 mL) was introduced into a teflon-lined autoclave and heated at 220 °C for 72 h in an oven under static condition. The obtained Al-MIL-53 was purified twice in ethanol at 80 °C for 12 h and washed with ethanol. The synthesized sample was further dried overnight at 60 °C under dynamic vacuum.

2.1.2. Preparation of Al-O-C

Typically, 2.0 g Al-MIL-53 was placed in a porcelain boat and charged into a flow-through tube furnace. The furnace was heated to 800 °C under a argon atmosphere with a heating rate of 5 °C/min, and then maintained at the target temperature for 2 h, followed by cooling down to room temperature in a argon atmosphere. The obtained solid was immersed in 50 mL aqueous solution of NaOH (0.5 M) and 5 mL ethanol and stirred at room temperature for 12 h. The final product was collected by centrifugation and washed 3 times with de-ionized water and ethanol. The resultant product was further dried overnight at 60 °C under dynamic vacuum. The inductively coupled plasma-atomic emission spectroscopyinductively (ICP-AES) result indicates the actual Al content is 5.3 wt%.

2.1.3. Preparation of Al-O-C-P and Al-O-C-L

Typically, Al-O-C (400 mg) were immersed in 20 mL aqueous solution of NaOH (0.5 M) and 2 mL ethanol and stirred at room temperature for 6 h and 12 h to give Al-O-C-P and Al-O-C-L, respectively. The final products were collected by centrifugation and washed 3 times with de-ionized water and ethanol. The resultant products were further dried overnight at 60 °C under dynamic vacuum. The ICP-AES result indicates the actual Al content in Al-O-C-P and Al-O-C-L are 3.3 wt% and 1.4 wt%, respectively.

2.1.4. Preparation of bulk PILs

Typically, a mixture of 1,2-divinylbenzene (DVB, 60 μL), 1-vinyl-3-ethylimidazolium bromide (VEI-Br, 100 mg), 2,2′-azobis-isobutyronitrile (AIBN, 3 mg) and ethanol (400 μL) was placed into a flask (10 mL), and a balloon filled with nitrogen was connected to the flask [54]. The flask was purged with nitrogen for several times. Afterward, the mixture was sonicated for 10 min and heated to 70 °C for 24 h under nitrogen protection. Finally, the obtained product was washed with ethanol for several times, and dried overnight at 60 °C under dynamic vacuum.

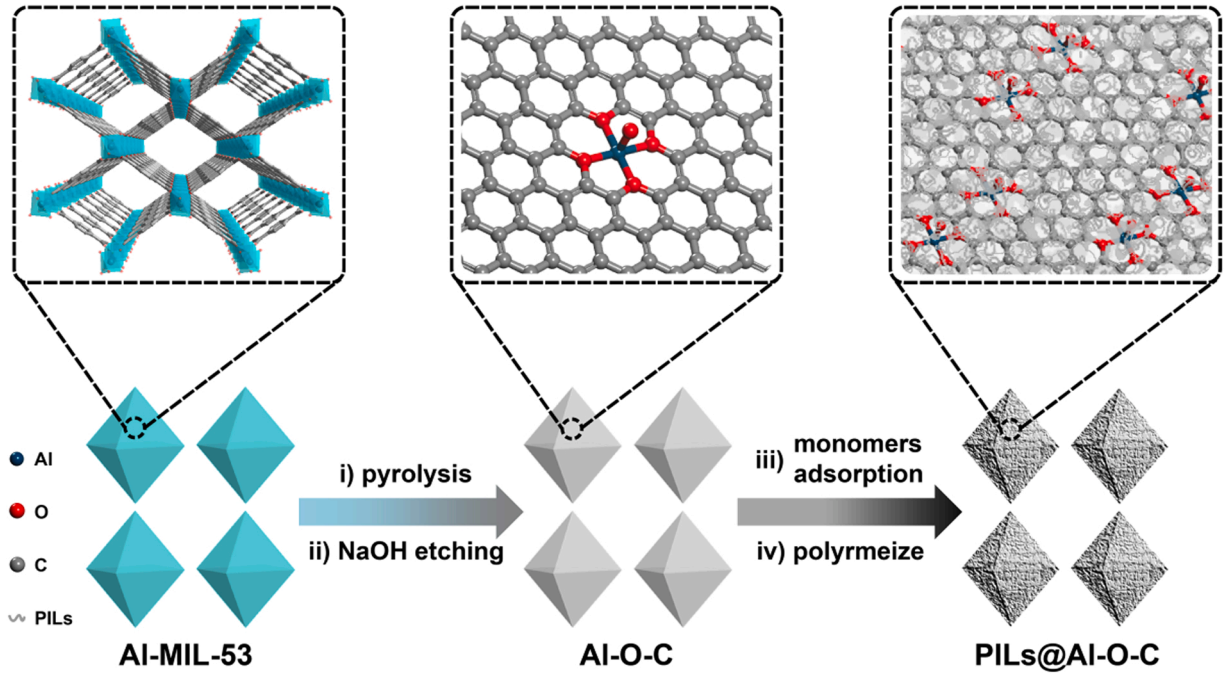

Scheme 1. Schematic illustration of the rational fabrication of PILs@Al-O-C catalyst.

2.1.5. Preparation of PILs@Al-O-C and PILs@Al-O-C-X (X = P or L)

Typically, Al-O-C (100 mg) or Al-O-C-X (100 mg) was mixed with a mixture of VEI-Br (100 mg), DVB (60 μL), AIBN (3 mg) and ethanol (400 μL) in a flask (10 mL), and a balloon filled with nitrogen was connected to the flask. The flask was purged with nitrogen for several times. Afterward, the mixture was sonicated for 10 min and heated to 70 °C for 24 h under nitrogen protection. Finally, the obtained product was washed with ethanol for several times, and dried overnight at 60 °C under dynamic vacuum.

2.2. Catalytic activity characterization

Generally, a mixture of catalysts and 20 mmol epoxide was placed into a flask and a balloon filled with CO_2 was connected to the flask. The reactor was purged with CO_2 for several times. The catalytic cycloaddition reaction was carried out at target temperature (80 °C or 110 °C). After the reaction, the yield of target product was detected by GC (see Section 2 in Supplementary Material for details).

2.3. Density functional theory (DFT) calculations

DFT calculations are performed by using the Vienna ab-initio Simulation Package (VASP-5.4) to optimize all the geometry structures and energies (see Section 3 in Supplementary Material for details).

3. Results and discussion

3.1. Characterizations of PILs@Al-O-C

Powder X-ray diffraction (XRD) pattern and scanning electron microscopy (SEM) observation show that Al-MIL-53 with high crystallization and regular morphology was successfully prepared (Fig. 1a and Fig. S1). Upon pyrolysis at 800 °C and subsequent alkaline etching process, Al-MIL-53 can be converted to the Al-O-C sample without any identifiable metallic particle (Fig. 1b). Following that, VEI-Br and DVB as the monomers of PILs were introduced into the pores of Al-O-C, and the PILs@Al-O-C catalyst was generated via the in-situ polymerization initiated by adding AIBN at 70 °C.

To our delight, the powder XRD pattern of PILs@Al-O-C is similar to that of Al-O-C and no identifiable diffraction peaks related to Al-based phase (e.g., Al or Al_2O_3) can be detected (Fig. 1b). Moreover, the Raman scattering spectrum of PILs@Al-O-C gives comparable intensity ratio of D band (~1340 cm^{-1}) and G band (~1590 cm^{-1}) to that of Al-O-C, indicating the carbon matrix of Al-O-C was well retained during the polymerization process (Fig. 1c). To verify whether the polymerization of two monomers (i.e., DVB and VEI-Br) was carried out in Al-O-C, a comparative synthesis experiment with the product of bulk PILs was conducted under similar conditions in the absence of Al-O-C (Fig. S2). The Fourier transform infrared (FTIR) spectrum of PILs@Al-O-C exhibits typical characteristic peaks at ~1160 and ~1446 cm^{-1}, corresponding to the C-N stretching vibration and bending vibration of the imidazolium ring in the bulk PILs network [55,56], respectively (Fig. 1d), manifesting the successful introduction of PILs into the Al-O-C framework.

The loading impact of PILs on the porosity of Al-O-C was investigated by the N_2 sorption at 77 K (Fig. 2a), which demonstrates that the Brunauer-Emmett-Teller (BET) surface area and pore volume for PILs@Al-O-C drops to 332 m^2/g and 0.47 cm^3/g, respectively, compared with Al-O-C (BET: 741 m^2/g, pore volume: 0.72 cm^3/g). The appreciable decrease in surface area and pore volume for PILs@Al-O-C can be attributed to the increased weight from the PILs or/and the

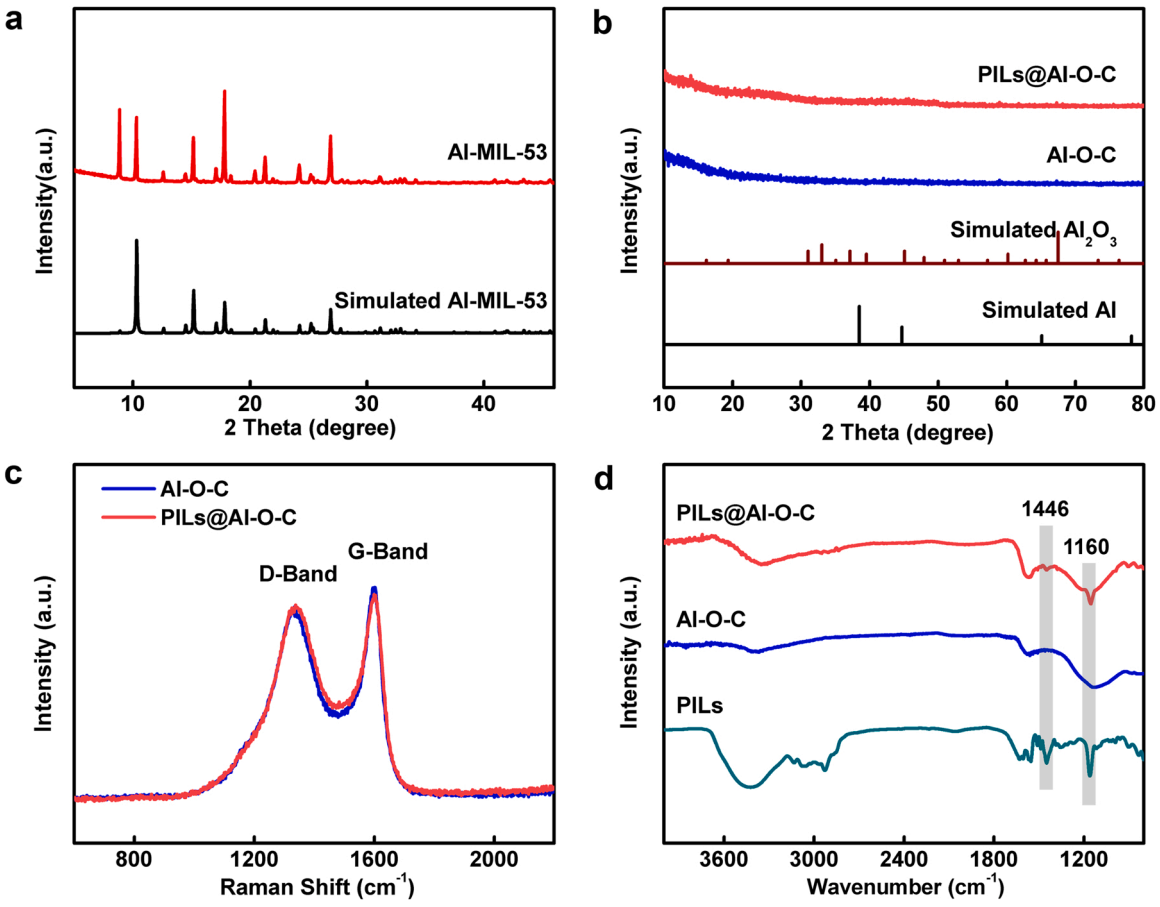

Fig. 1. (a) Powder XRD patterns for simulated Al-MIL-53 and synthesized Al-MIL-53. (b) Powder XRD patterns for simulated Al, simulated Al_2O_3, synthesized Al-O-C and PILs@Al-O-C. (c) The Raman spectra of Al-O-C and PILs@Al-O-C. (d) FTIR spectra of bulk PILs, Al-O-C and PILs@Al-O-C.

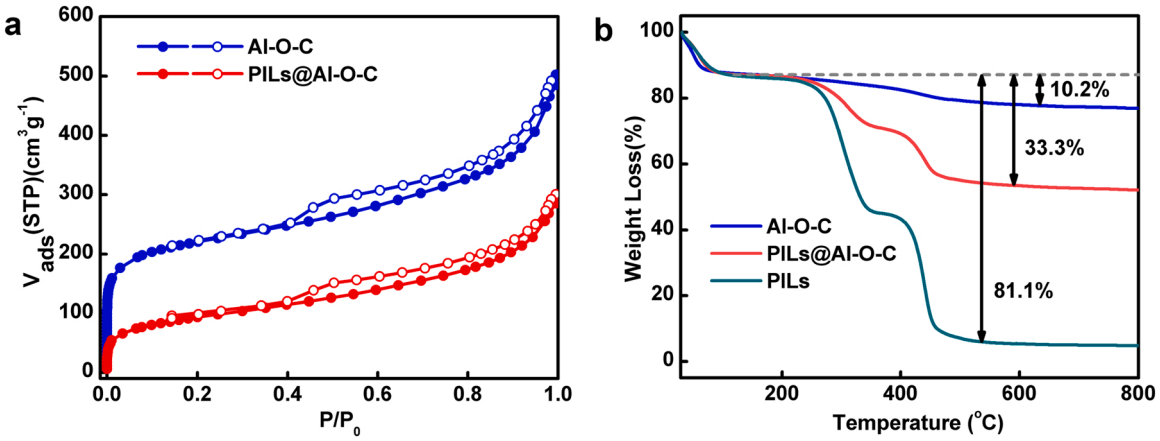

Fig. 2. (a) N_2 sorption isotherms for Al-O-C and PILs@Al-O-C at 77 K. (b) TGA plots of bulk PILs, Al-O-C and PILs@Al-O-C.

occupation effect of PILs located in the cavities of Al-O-C. The pore size distribution of PILs@Al-O-C shows that the percentage of pores with diameters greater than 10 nm is significantly reduced, while the dominate pores centered about 5 nm are well conserved (Fig. S3), suggesting the polymerization of PILs was mainly carried out in the cavities with bigger diameters. Notably, the mesopores (~5 nm) maintained in PILs@Al-O-C is beneficial for the transport of substrates/products, and the narrow pore sizes might enhance the CO_2 enrichment capability. The thermo-gravimetric analysis (TGA) curves for bulk PILs and PILs@Al-O-C are qualitatively similar and present two weight loss steps (Fig. 2b), which further demonstrates the successful incorporation of PILs in the Al-O-C matrix. According to the weight loss percentages, the loading amount of PILs in PILs@Al-O-C is ~32 wt% (see Section 4 in Supplementary Material for calculation details), consistent with the result of elemental analysis (Table S1).

As expected, the morphology of PILs@Al-O-C was similar to that of Al-O-C, and no identifiable spongy structure attribute to bulk PILs can be observed on the surface, indicating that the generation of PILs is mostly carried out in the cavities of Al-O-C (Fig. 3a and Fig. S4). The transmission electron microscopy (TEM) image reveals that PILs@Al-O-C

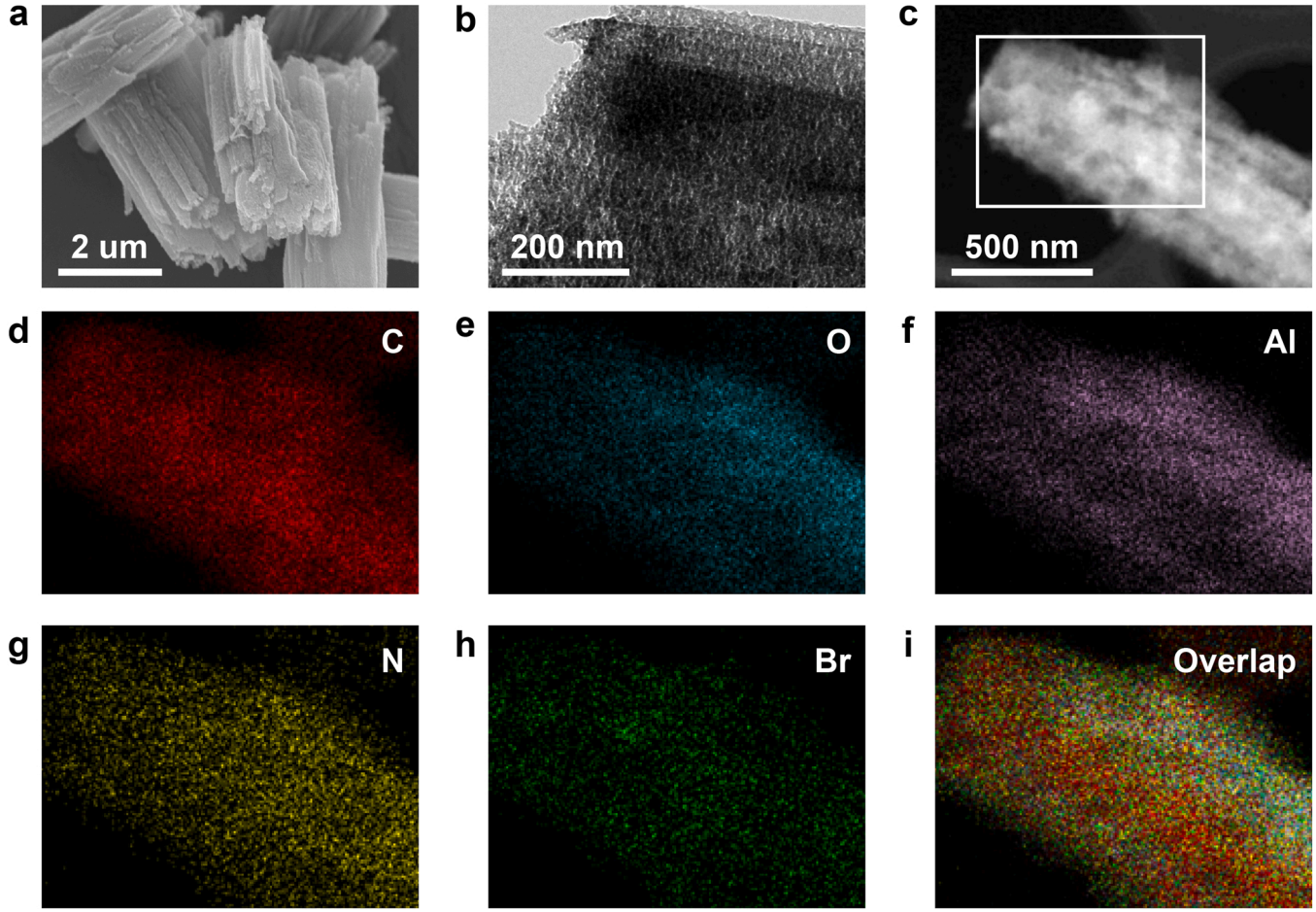

Fig. 3. (a) SEM image, (b) TEM image and (c) HAADF-STEM image of PILs@Al-O-C. The elemental mapping of (d) C, (e) O, (f) Al, (g) N (h) Br and (i) overlap for the selected area in (c).

possesses abundant narrow mesopores (Fig. 3b), which is in good agreement with the afore-mentioned analysis of pore size distribution (Fig. S3). Moreover, the elemental mapping result reveals that the PILs@Al-O-C is composed of Al, O, C, N, Br, among which N and Br from PILs are well distributed throughout the Al-O-C matrix (Fig. 3c–i), further highlighting that the polymerization of PILs should be occurred in the cavities of Al-O-C, instead of being coated on the Al-O-C surface. Moreover, the high-resolution TEM (HRTEM) observation shows that no Al or Al_2O_3 particles can be observed (Fig. S5). It is demonstrated that only atomically dispersed Al species can be identified in randomly selected areas (Fig. 4a and Fig. S6) over aberration-corrected high-angle annular dark-field scanning TEM (HAADF-STEM).

To unveil the existence status of Al-involved species in PILs@Al-O-C, X-ray absorption spectroscopy (XAS), a powerful technique to determine the electronic and structural information of the target species was adopted. As shown in the X-ray absorption near-edge structure (XANES) spectra, the energy absorption threshold of PILs@Al-O-C is located between that of Al_2O_3 and Al foil (Fig. 4b), illustrating the existence of positively charged $Al^{\delta+}$ sites ($0 < \delta < 3$) in PILs@Al-O-C. The extended X-ray absorption fine structure (EXAFS) spectrum of PILs@Al-O-C at Al K-edge only exhibits one main peak at ~1.4 Å, assigning to the Al-O scattering paths, and no fingerprinting signal peaks of Al-Al bond in Al_2O_3 (~ 2.4 Å) and Al foil (~ 2.3 Å) were detected, indicating the formation of atomically dispersed Al sites in PILs@Al-O-C (Fig. 4c). The best fitting result of the obtained EXAFS data of PILs@Al-O-C reveals that each Al atom is coordinated by ~5 oxygen atoms in average (Fig. 4d, Fig. S7 and Table S2). The AlO_5 motifs with unsaturated coordinated Al sites in PILs@Al-O-C can be employed as the Lewis acid sites to catalyze CO_2 cycloaddition reactions.

3.2. Catalytic performance of PILs@Al-O-C towards CO_2 cycloaddition

Epichlorohydrin, a typical industrial epoxide [57], was first selected as a model compound to explore the optimized reaction parameters. As expect, PILs@Al-O-C possesses the highest catalytic yield (~91%) with 1 bar CO_2 at 80 °C in the absence of solvent and co-catalyst (Fig. 5a). In contrast, the production of target product (i.e., chloropropene carbonate) was undetectable when 1 bar CO_2 was replaced by 1 bar N_2 with other reaction parameters unchanged, revealing that the C1 source of cyclic carbonate comes from CO_2 rather than the decomposition of catalyst. Compared with PILs@Al-O-C, the yield of target product sharply drops to ~3% and ~64% over Al-O-C and PILs, respectively, under similar conditions (Fig. 5a), which unequivocally indicates the synergistic effect between the atomically dispersed Al sites and well-distributed PILs network. Although the physical mixtures of Al-O-C catalyst with bromine-containing monomer (VEI-Br) or TBAB give ~95% yields, the superior solubility of VEI-Br and TBAB is unfavorable for separation from the catalytic system. Moreover, the controlled experiment with the counterpart of physically mixed Al-O-C and PILs (denoted as Al-O-C+PILs) was conducted, and only 75% target product was detected (Fig. 5a), which might be due to the limited active sites available in bulk PILs with inferior surface area (Fig. S8), or/and mass diffusion transport resistance caused by spatially separated active sites.

In order to evaluate the significance of atomically disperded Lewis acid sites (i.e., atomically dispersed Al sites), the contents of Al in PILs@Al-O-C were partially or largely removed to give PILs@Al-O-C-P

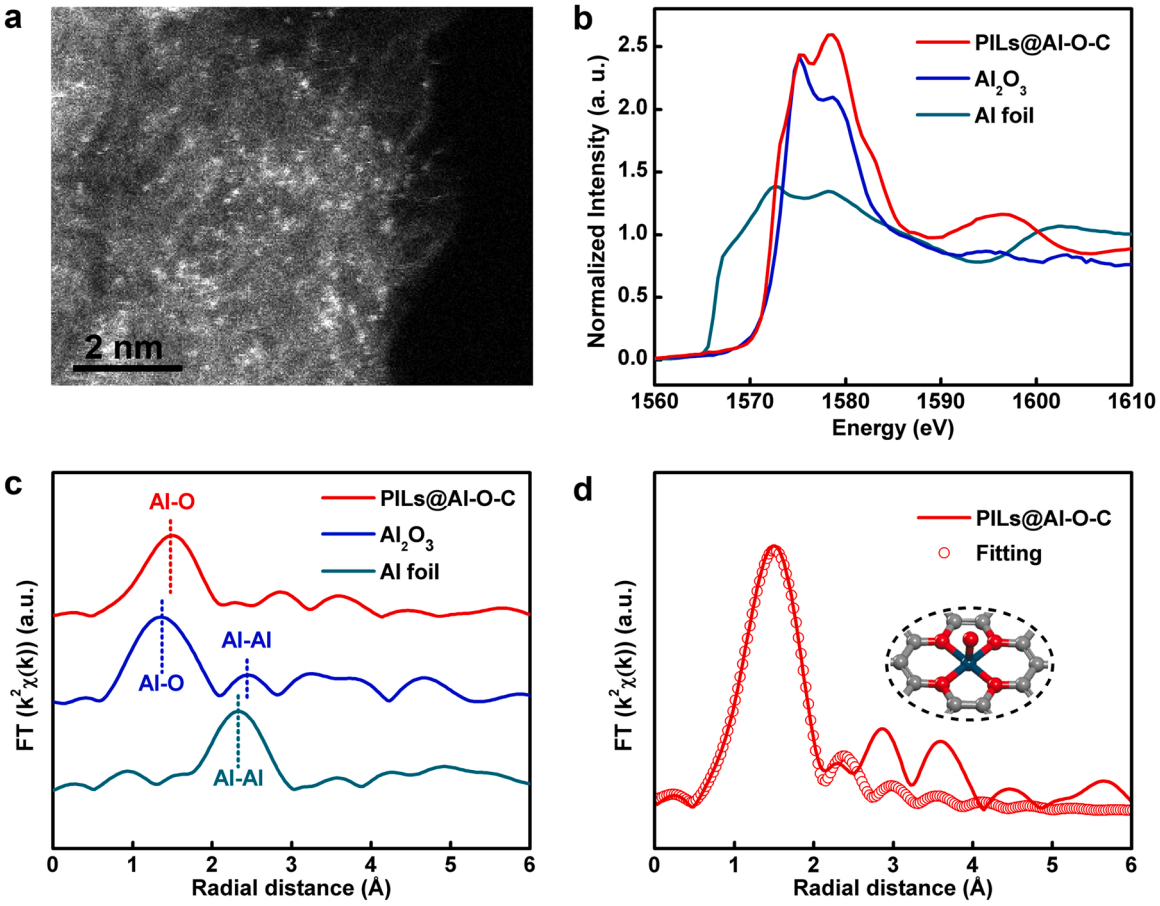

Fig. 4. (a) Aberration corrected HADDF-STEM image of PILs@Al-O-C. (b) Al K-edge XANES spectra and (c) Fourier transform of EXAFS spectra of PILs@Al-O-C, Al_2O_3 and Al foil. (d) EXAFS fitting curve of Al species in PILs@Al-O-C (inset: schematic model of atomically dispersed Al species; the blue, red and grey spheres represent Al, O and C atoms, respectively).

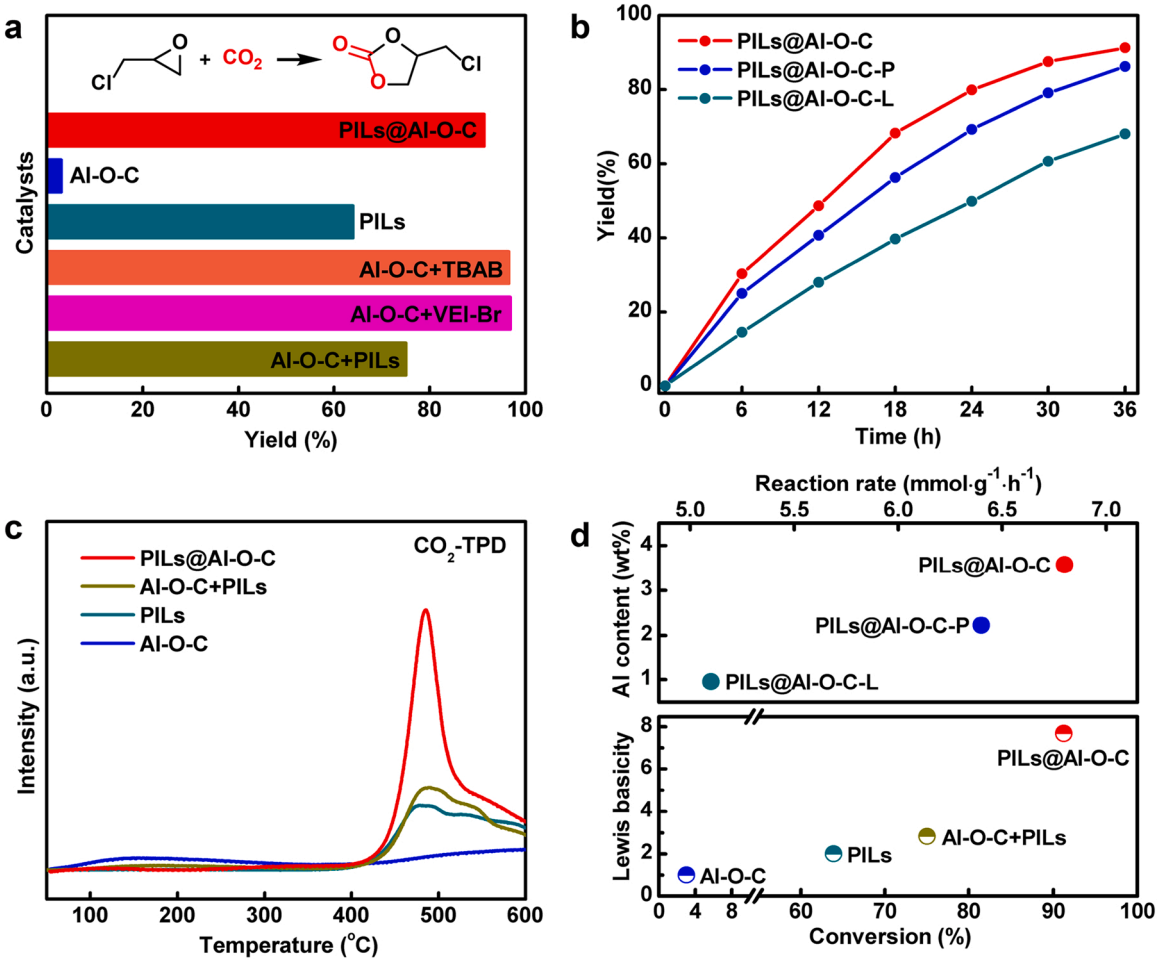

Fig. 5. (a) Catalytic yields of CO_2 cycloaddition with epichlorohydrin over various as-prepared catalysts in the absence of solvent and co-catalyst. (b) Catalytic performance comparison for cycloaddition reaction of CO_2 and epichlorohydrin in the present of PILs@Al-O-C, PILs@Al-O-C-L and PILs@Al-O-C-H, respectively. (c) CO_2-TPD profiles of PILs@Al-O-C, Al-O-C+PILs, PILs and Al-O-C. (d) The correlation of catalytic performance with (up) Al content and (down) the Lewis basicity of catalysts.

(Al: 2.23 wt%) and PILs@Al-O-C-L (Al: 0.95 wt%), respectively. As shown in Fig. 5b, the catalytic activity is positively correlated with the concentration of Al species in catalysts, illustrating that the atomically disperded Lewis acid sites are helpful to the CO_2 cycloaddition reaction. Furthermore, the activation energy (Ea) for CO_2 cycloaddition with epichlorohydrin over PILs was determined to be 75.6 kJ mol^{-1} (see Section 5 in Supplementary Material for details) [58–60], which was sharply reduced to 53.0 kJ mol^{-1} with the utilization of PILs@Al-O-C (Fig. S9), which further demonstrates the significant importance of atomically disperded Lewis acid sites for CO_2 cycloaddition reaction. In addition, the Lewis basicity of PILs@Al-O-C was evaluated by the temperature programmed desorption of CO_2 (CO_2-TPD). Compared with Al-O-C, a narrow peak with enhanced intensity in the high temperature range, assigning to the chemisorption peak of CO_2 [61], was observed in CO_2-TPD profile of PILs@Al-O-C (Fig. 5c), which validates that the incorporation of PILs endows PILs@Al-O-C with stronger Lewis basicity and thus enhances the catalytic performance of CO_2 cycloaddition. Notably, the intensity of CO_2 desorption peak in the CO_2-TPD profile of PILs@Al-O-C is higher than those of PILs and Al-O-C+PILs with the same amount of PILs (Fig. 5c), which might be due to the fact that the uniformly dispersed PILs network in PILs@Al-O-C can expose more available Lewis base sites than that of bulk PILs with inferior surface area (Fig. S8). On the basis of above information, we believe that the uniform Lewis acid sites and abundant Lewis base sites synergistically promote the catalytic performance towards CO_2 cycloaddition with epichlorohydrin (Fig. 5d).

The filtration test demonstrated that the increase of target product is negligible even after 30 h upon the catalyst removal while other conditions remain (Fig. 6a), which is significantly different from the filtration result over the physically mixed catalyst composed of Al-O-C and TBAB (Fig. 6b), reflecting the heterogeneous catalytic nature of PILs@Al-O-C. Moreover, to examine whether the halogen anions (i.e., Br^-) would be leached from the PILs@Al-O-C during the catalytic reaction, the content of Br^- in the solution after reaction was detected by adding $AgNO_3$. Compared with the precipitates formed in TBAB and VEI-Br solutions after adding $AgNO_3$ solution, no obvious change was observed in the solution from PILs@Al-O-C (Fig. S10), revealing that the leaching of Br^- anions almost does not occur during the catalytic reaction over PILs@Al-O-C. The morphology and superior catalytic performance of PILs@Al-O-C is well maintained during the 5 cycles (Fig. 7a and Fig. S11). The Powder XRD pattern, Raman scattering spectrum and FTIR spectrum for PILs@Al-O-C after reaction are similar to those before the reaction and no identifiable particles of Al or Al_2O_3 can be observed in the HRTEM image (Fig. S12-S15), indicating the excellent stability of PILs@Al-O-C. In order to investigate the catalytic performance of PILs@Al-O-C under low CO_2 pressure, a mixture gas containing 0.25 bar CO_2 and 0.75 bar N_2 was employed for the cycloaddition reaction. Delightedly, the excellent yield (>90%) of target product can be achieved by extending the reaction time (Fig. S16).

Encouraged by the excellent catalytic activity of PILs@Al-O-C

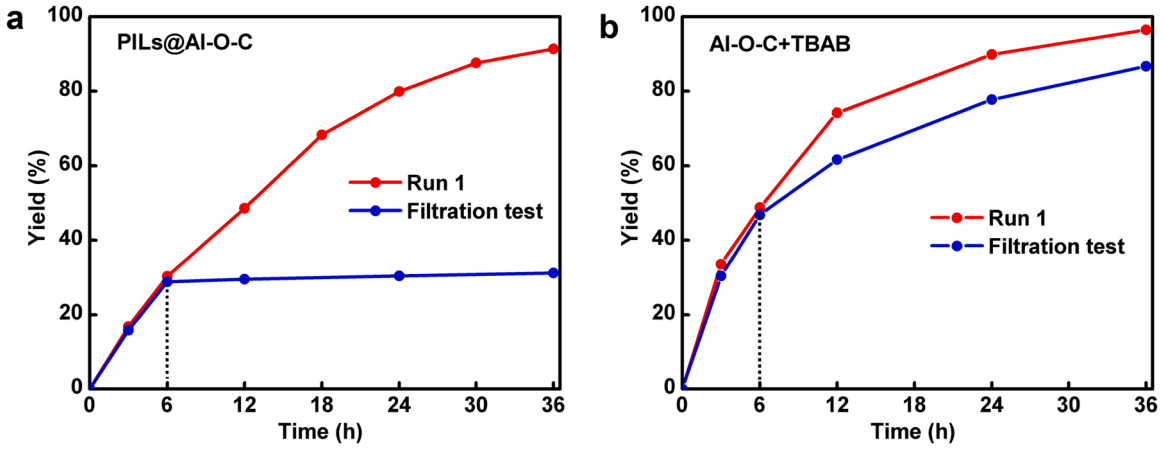

Fig. 6. Filtration tests of cycloaddition reaction of CO_2 and epichlorohydrin over (a) PILs@Al-O-C and (b) the physical mixture of Al-O-C and TBAB.

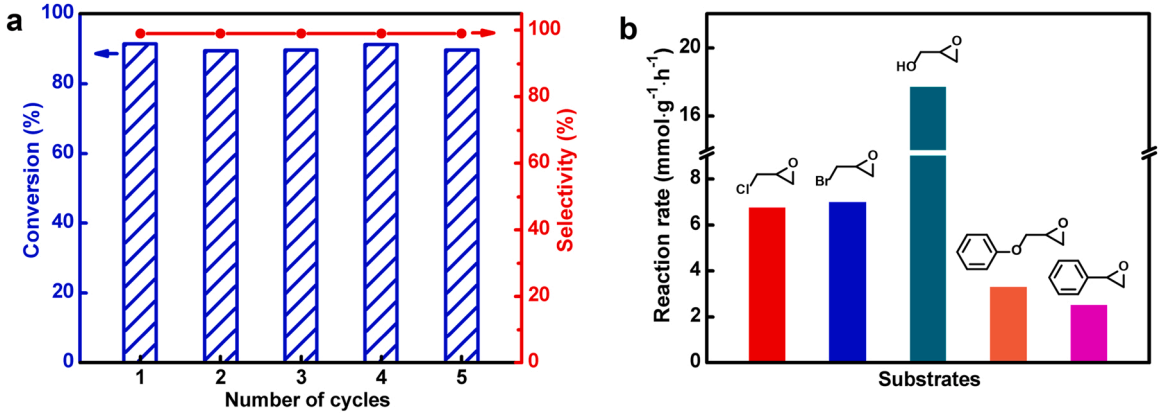

Fig. 7. (a) Catalytic recyclability of PILs@Al-O-C for CO_2 cycloaddition with epichlorohydrin. (b) Catalytic performance comparison of PILs@Al-O-C towards the CO_2 cycloaddition with different epoxides.

towards the CO_2 cycloaddition with epichlorohydrin, various epoxides with different substituents have also been investigated. As summarized in Fig. 7b and Table S3, all small epoxides with electron-withdrawing groups (-Cl and -Br) or electron-donating substituents (-OH) can be quickly converted to corresponding products with good to high yields in the present of PILs@Al-O-C, while the catalytic reaction rate of glycidol is ~2.5 times higher than that of epichlorohydrin. In the case of epichlorohydrin, the electron-withdrawing group (i.e., -Cl) leads the α-carbon to be less negatively charged than that of β-carbon, and thus, the nucleophilic attack of Br^- anions on the α-carbon is more favorable [62]. However, the nucleophilic attack on the α-carbon would be disturbed owing to the steric effect of substituent, forcing the nucleophilic attack to occur on the less reactive β-carbon but without steric hindrance. In contrast, the glycidol with electron-donating group (i.e., -OH) makes the α-carbon to be more negatively charged than that of β-carbon, and enables the nucleophilic attack to proceed on the active β-carbon without steric hindrance. More importantly, glycidol can also serve as the catalyst for the cycloaddition reaction of CO_2 with itself [63], thereby significantly enhancing the catalytic activity. The relatively low catalytic efficiencies toward 2-(phenoxymethyl)-oxirane and styrene oxide can be owing to the steric hindrance effect of their large substituent.

3.3. Catalytic mechanism of PILs@Al-O-C towards CO_2 cycloaddition

To gain more insights into the synergistic effect of PILs and atomically dispersed Al sites for the cycloaddition reaction of CO_2 and epoxides, the density functional theory (DFT) calculations were conducted to explore the whole catalytic process. As shown in Fig. 8a, a graphene sheet-based model with the five coordinated Al-O_5 structure was constructed by connecting OH group to the planar AlO_4 unit along the axial direction to satisfy the AlO_5 motif in the PILs@Al-O-C. For the cycloaddition reaction of CO_2 and epichlorohydrin over Al-O-C (Fig. 8b), the oxygen atom in epichlorohydrin is initially adsorbed on the Lewis site (Al) with the distance (D_{Al-O}) of 3.17 Å. When CO_2 approaches the adsorbed epichlorohydrin, the linearly O═C═O gradually bents with an angle of ∠147° to form the transition state. The C atom in bended CO_2 will strongly interact with O of epichlorohydrin and push it away from Al (D_{Al-O} = 3.39 Å), among which high energy (~179 kJ·mol^{-1}) is required to overcome the energy barrier for the synthesis of cyclic carbonate (Fig. 8b).

As a comparison, the DFT calculation for CO_2 cycloaddition with epichlorohydrin in the presence of PILs@Al-O-C was also conducted (Fig. 8c-d). It is noticeable that the intrinsic Br^- of the imidazolium-based PILs is active enough to open the C-O-C ring in the epichlorohydrin (i.e., ring-opening step) with releasing energy of ~100 kJ·mol^{-1} (Fig. 8c). At the following CO_2 insertion step (i.e., rate-limiting step), the linear O═C═O was attacked by the ring-opened intermediate with overcoming an energy barrier of ~149 kJ mol^{-1}. The subsequent intramolecular cyclization (i.e., ring-closing step) proceeds readily to afford the cyclic carbonate with an energy barrier value of ~65 kJ mol^{-1}. Finally, the desorption process of target product is endothermic with an energy barrier value of ~93 kJ mol^{-1}, meanwhile, the catalyst is regenerated. Compared with the high energy barrier

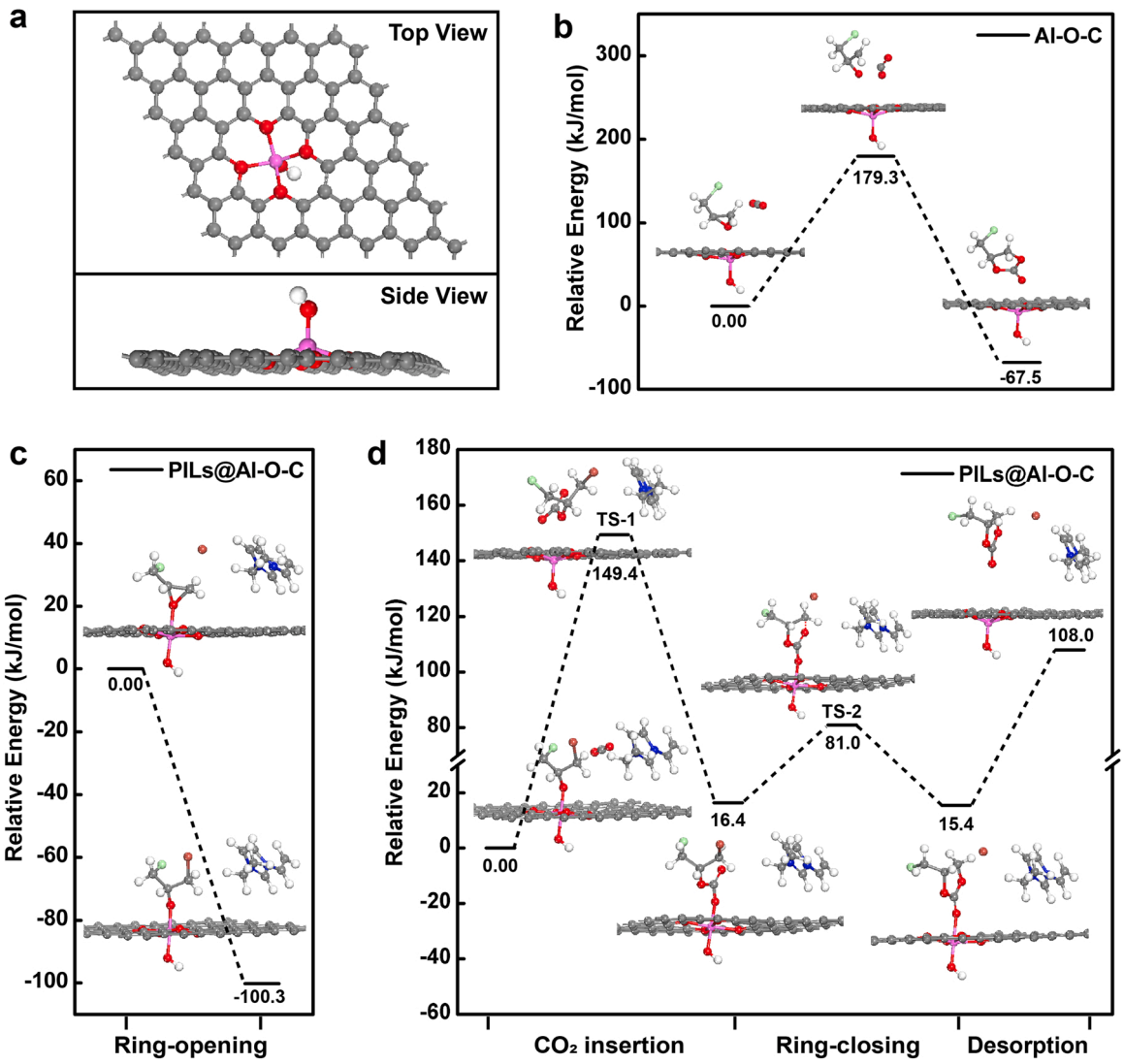

Fig. 8. (a) Simulated Al-O-C model. (b) Relative Gibbs energy of CO_2 cycloaddition with epichlorohydrin over Al-O-C. Relative Gibbs energy of (c) the ring-opening step and (d) the CO_2-containing steps for cycloaddition reaction of CO_2 and epichlorohydrin in the present of PILs@Al-O-C. The pink, red, gray, white, blue, green and brown balls in Fig. 8b–d represent Al, O, C, H, N, Cl and Br atoms, respectively. The enlarged pictures and corresponding cartesian coordinates of the optimized structures inserted in Fig. 8c-d were provided in the attachment page in Supplementary Material.

(~179 kJ mol^{-1}) of Al-O-C system, the energy barrier reduces to ~149 kJ mol^{-1} with the existence of PILs@Al-O-C, meaning that the reaction rate constant of PILs@Al-O-C, determined by the Eyring equation [64], is ~27,000 times higher than that of Al-O-C (see Section 6 in Supplementary Material for calculation details), which can be the main account for the enhanced catalytic performance observed in experiment. Moreover, combined with the previous exothermic ring-opening step (~100 kJ mol^{-1}), the actual energy requirement for overcoming the energy barrier of CO_2 cycloaddition with epichlorohydrin could be further reduced in the presence of PILs@Al-O-C, which might be the another reason for the improvement of catalytic activity.

4. Conclusions

In summary, we have rationally fabricated a PILs@Al-O-C catalyst with atomically dispersed Al species (i.e., AlO_5, Al: ~3.58 wt%) and uniformly distributed PILs networks for catalytic CO_2 cycloaddition with epoxides, among which the AlO_5 motifs served as Lewis acid sites to promote the activation of epoxides, and the high content of Br^- ions (i.e., nucleophilic agents) stabilized by imidazolium-based frame in PILs cooperate to accelerate the ring opening of epoxides. Meanwhile, the high density of N atoms in PILs network and the porous character of carbon-based matrix facilitate the CO_2 enrichment and rapid transport of substrates/products, respectively. As a result, the PILs@Al-O-C presents excellent catalytic performance towards CO_2 cycloaddition reaction without the assistance of solvent and co-catalyst. More importantly, the superior activity of PILs@Al-O-C are well maintained during the 5 recycling experiments. This work not only represents the first attempt on integration of atomically dispersed Lewis acid sites and immobilized ionic liquids into CO_2 cycloaddition reaction, but also opens an avenue in development of multifunctional and recyclable heterogeneous catalysts for CO_2 fixation.

CRediT authorship contribution statement

Qihao Yang, Zhiyi Lu and Honglin Gao: designed the project and wrote the manuscript. **Huaitao Peng and Yinming Wang:** carried out the experiments and collected the data. **Qiu Yang:** made a great contribution on ex-situ characterizations (i.e., SEM, XRD and HRTEM). **Qiuju Zhang:** carried out DFT calculations and wrote the computational part of the manuscript. **Nian Zhang, Jing Zhou and Linjuan Zhang:** performed the XANES and EXAFS experiments and data analysis.

Declaration of Competing Interest

The authors declare the following financial interests/personal relationships which may be considered as potential competing interests: Qihao Yang, Honglin Gao, Jing Zhou, Linjuan Zhang reports financial support was provided by National Natural Science Foundation of China. Qihao Yang reports financial support was provided by Zhejiang Provincial Natural Science Foundation of China. Qiuju Zhang, Linjuan Zhang, Qihao Yang, Zhiyi Lu reports financial support was provided by Chinese Academy of Sciences. Zhiyi Lu reports financial support was provided by Ningbo Yongjiang Talent Introduction Programme. Qiuju Zhang, Linjuan Zhang reports financial support was provided by K. C. Wong Education Foundation. Zhiyi Lu reports financial support was provided by Ningbo S&T Innovation 2025 Major Special Program. Qihao Yang reports financial support was provided by Ningbo Natural Science Foundation. Linjuan Zhang reports equipment, drugs, or supplies was provided by Transformational Technologies for Clean Energy and Demonstration.

Acknowledgment

This work is supported by the National Natural Science Foundation of China, China (22101288, 21876183, 21905295, 22179141 and 21865039), the Zhejiang Provincial Natural Science Foundation of China, China (LQ22B010005 and LY21B030006), the “From 0 to 1″ Innovative Program of Chinese Academy of Sciences, China (ZDBS-LY-JSC021), the Hundred Talents Programs in Chinese Academy of Sciences, the Ningbo Yongjiang Talent Introduction Program, China (2021A-036-B), the Ningbo S&T Innovation 2025 Major Special Program, China (2020Z059 and 2020Z107), the Science and Technology Innovation 2025 Program in Ningbo, China (2019B10046), the Ningbo Natural Science Foundation, China (2021J202), the K.C. Wong Education Foundation, China (GJTD-2019-13 and GJTD-2018-10), the Strategic Priority Research Program of the Chinese Academy of Sciences, China (XDA21000000), the DNL Cooperation Fund, CAS, China (DNL202008), the Youth Innovation Promotion Association, Chinese Academy of Sciences, China (Y201842) and the “Transformational Technologies for Clean Energy and Demonstration, China”.

Declaration of Competing Interest

The authors declare that they have no known competing financial interests or personal relationship that could have appeared to influence the work reported in this paper.

Appendix A. Supporting information

Supplementary data associated with this article can be found in the online version at doi:10.1016/j.apcatb.2022.121463.

References

[1] A.M. Appel, J.E. Bercaw, A.B. Bocarsly, H. Dobbek, D.L. DuBois, M. Dupuis, J. G. Ferry, E. Fujita, R. Hille, P.J. Kenis, C.A. Kerfeld, R.H. Morris, C.H. Peden, A. R. Portis, S.W. Ragsdale, T.B. Rauchfuss, J.N. Reek, L.C. Seefeldt, R.K. Thauer, G. L. Waldrop, Frontiers, opportunities, and challenges in biochemical and chemical catalysis of CO_2 fixation, Chem. Rev. 113 (2013) 6621–6658.

[2] A. Chen, B.-L. Lin, A simple framework for quantifying electrochemical CO_2 fixation, Joule 2 (2018) 594–606.

[3] M. Ding, R.W. Flaig, H.L. Jiang, O.M. Yaghi, Carbon capture and conversion using metal-organic frameworks and MOF-based materials, Chem. Soc. Rev. 48 (2019) 2783–2828.

[4] S. Das, J. Perez-Ramirez, J. Gong, N. Dewangan, K. Hidajat, B.C. Gates, S. Kawi, Core-shell structured catalysts for thermocatalytic, photocatalytic, and electrocatalytic conversion of CO_2, Chem. Soc. Rev. 49 (2020) 2937–3004.

[5] L. Zhang, Z. Han, X. Zhao, Z. Wang, K. Ding, Highly efficient ruthenium-catalyzed N-formylation of amines with H_2 and CO_2, Angew. Chem. Int. Ed. 54 (2015) 6186–6189.

[6] X. Zhang, X. Li, D. Zhang, N.Q. Su, W. Yang, H.O. Everitt, J. Liu, Product selectivity in plasmonic photocatalysis for carbon dioxide hydrogenation, Nat. Commun. 8 (2017) 14542.

[7] L. Wang, W. Zhang, X. Zheng, Y. Chen, W. Wu, J. Qiu, X. Zhao, X. Zhao, Y. Dai, J. Zeng, Incorporating nitrogen atoms into cobalt nanosheets as a strategy to boost catalytic activity toward CO_2 hydrogenation, Nat. Energy 2 (2017) 869–876.

[8] R. Sen, A. Goeppert, S. Kar, G.K.S. Prakash, Hydroxide based integrated CO_2 capture from air and conversion to methanol, J. Am. Chem. Soc. 142 (2020) 4544–4549.

[9] J. Zhu, T. Diao, W. Wang, X. Xu, X. Sun, S.A.C. Carabineiro, Z. Zhao, Boron doped graphitic carbon nitride with acid-base duality for cycloaddition of carbon dioxide to epoxide under solvent-free condition, Appl. Catal. B: Environ. 219 (2017) 92–100.

[10] G. Zhai, Y. Liu, Y. Mao, H. Zhang, L. Lin, Y. Li, Z. Wang, H. Cheng, P. Wang, Z. Zheng, Y. Dai, B. Huang, Improved photocatalytic CO_2 and epoxides cycloaddition via the synergistic effect of Lewis acidity and charge separation over Zn modified UiO-bpydc, Appl. Catal. B: Environ. 301 (2022), 120793.

[11] Y. Liu, D. Deng, X. Bao, Catalysis for selected C1 chemistry, Chem 6 (2020) 2497–2514.

[12] Y. Yin, B. Hu, X. Li, X. Zhou, X. Hong, G. Liu, Pd@zeolitic imidazolate framework-8 derived PdZn alloy catalysts for efficient hydrogenation of CO_2 to methanol, Appl. Catal. B: Environ. 234 (2018) 143–152.

[13] J. Lin, C. Ma, Q. Wang, Y. Xu, G. Ma, J. Wang, H. Wang, C. Dong, C. Zhang, M. Ding, Enhanced low-temperature performance of CO_2 methanation over mesoporous Ni/Al_2O_3-ZrO_2 catalysts, Appl. Catal. B: Environ. 243 (2019) 262–272.

[14] L.-L. Ling, W. Yang, P. Yan, M. Wang, H.-L. Jiang, Light-assisted CO_2 hydrogenation over Pd_3Cu@UiO-66 promoted by active sites in close proximity, Angew. Chem. Int. Ed. 61 (2022), e20211639.

[15] S.S.A. Shah, T. Najam, M. Wen, S.-Q. Zang, A. Waseem, H.-L. Jiang, Metal-organic framework-based electrocatalysts for CO_2 reduction, Small Struct. (2021), 2100090.

[16] Y. Xi, Y. Zhang, X. Cai, Z. Fan, K. Wang, W. Dong, Y. Shen, S. Zhong, L. Yang, S. Bai, PtCu thickness-modulated interfacial charge transfer and surface reactivity in stacked graphene/Pd@PtCu heterostructures for highly efficient visible-light reduction of CO_2 to CH_4, Appl. Catal. B: Environ. 305 (2022), 121069.

[17] T. Takahashi, T. Watahiki, S. Kitazume, H. Yasuda, T. Sakakura, Synergistic hybrid catalyst for cyclic carbonate synthesis: remarkable acceleration caused by immobilization of homogeneous catalyst on silica, Chem. Commun. (2006) 1664–1666.

[18] A. Rehman, V.C. Eze, M.F.M.G. Resul, A. Harvey, Kinetics and mechanistic investigation of epoxide/CO_2 cycloaddition by a synergistic catalytic effect of pyrrolidinopyridinium iodide and zinc halides, J. Energy Chem. 37 (2019) 35–42.

[19] A. Rehman, F. Saleem, F. Javed, H.G. Qutab, V.C. Eze, A. Harvey, Kinetic study for styrene carbonate synthesis via CO_2 cycloaddition to styrene oxide using silica-supported pyrrolidinopyridinium iodide catalyst, J. CO_2 Util. 43 (2021), 101379.

[20] J. Chen, H. Gao, T. Ding, L. Ji, J.Z.H. Zhang, G. Gao, F. Xia, Mechanistic studies of CO_2 cycloaddition reaction catalyzed by amine-functionalized ionic liquids, Front. Chem. 7 (2019) 615.

[21] B.-H. Xu, J.-Q. Wang, J. Sun, Y. Huang, J.-P. Zhang, X.-P. Zhang, S.-J. Zhang, Fixation of CO_2 into cyclic carbonates catalyzed by ionic liquids: a multi-scale approach, Green Chem. 17 (2015) 108–122.

[22] Y. Zhao, C. Yao, G. Chen, Q. Yuan, Highly efficient synthesis of cyclic carbonate with CO_2 catalyzed by ionic liquid in a microreactor, Green Chem. 15 (2013) 446–452.

[23] F.D. Bobbink, P.J. Dyson, Synthesis of carbonates and related compounds incorporating CO_2 using ionic liquid-type catalysts: state-of-the-art and beyond, J. Catal. 343 (2016) 52–61.

[24] T. Ema, Y. Miyazaki, J. Shimonishi, C. Maeda, J.Y. Hasegawa, Bifunctional porphyrin catalysts for the synthesis of cyclic carbonates from epoxides and CO_2: structural optimization and mechanistic study, J. Am. Chem. Soc. 136 (2014) 15270–15279.

[25] A. Decortes, A.M. Castilla, A.W. Kleij, Salen-complex-mediated formation of cyclic carbonates by cycloaddition of CO_2 to epoxides, Angew. Chem. Int. Ed. 49 (2010) 9822–9837.

[26] A.C. Deacy, A.F.R. Kilpatrick, A. Regoutz, C.K. Williams, Understanding metal synergy in heterodinuclear catalysts for the copolymerization of CO_2 and epoxides, Nat. Chem. 12 (2020) 372–380.

[27] L. Jiao, H.-L. Jiang, Metal-organic-framework-based single-atom catalysts for energy applications, Chem 5 (2019) 786–804.

[28] Q. Yang, W. Xu, S. Gong, G. Zheng, Z. Tian, Y. Wen, L. Peng, L. Zhang, Z. Lu, L. Chen, Atomically dispersed Lewis acid sites boost 2-electron oxygen reduction activity of carbon-based catalysts, Nat. Commun. 11 (2020) 5478.

[29] X. Yang, A. Wang, B. Qiao, J. Li, J. Liu, T. Zhang, Single-atom catalysts: a new frontier in heterogeneous catalysis, Acc. Chem. Res. 46 (2013) 1740–1748.

[30] L. Liu, A. Corma, Metal catalysts for heterogeneous catalysis: from single atoms to nanoclusters and nanoparticles, Chem. Rev. 118 (2018) 4981–5079.

[31] H. Zhang, G. Liu, L. Shi, J. Ye, Single-atom catalysts: emerging multifunctional materials in heterogeneous catalysis, Adv. Energy Mater. 8 (2018), 1701343.

[32] P. Yin, T. Yao, Y. Wu, L. Zheng, Y. Lin, W. Liu, H. Ju, J. Zhu, X. Hong, Z. Deng, G. Zhou, S. Wei, Y. Li, Single cobalt atoms with precise N-coordination as superior oxygen reduction reaction catalysts, Angew. Chem. Int. Ed. 55 (2016) 10800–10805.

[33] L. Lin, W. Zhou, R. Gao, S. Yao, X. Zhang, W. Xu, S. Zheng, Z. Jiang, Q. Yu, Y.W. Li, C. Shi, X.D. Wen, D. Ma, Low-temperature hydrogen production from water and methanol using Pt/alpha-MoC catalysts, Nature 544 (2017) 80–83.

[34] M. Kou, W. Liu, Y. Wang, J. Huang, Y. Chen, Y. Zhou, Y. Chen, M. Ma, K. Lei, H. Xie, P.K. Wong, L. Ye, Photocatalytic CO_2 conversion over single-atom MoN_2 sites of covalent organic framework, Appl. Catal. B: Environ. 291 (2021), 120146.
[35] P. Du, K. Hu, J. Lyu, H. Li, X. Lin, G. Xie, X. Liu, Y. Ito, H.-J. Qiu, Anchoring Mo single atoms/clusters and N on edge-rich nanoporous holey graphene as bifunctional air electrode in Zn-air batteries, Appl. Catal. B: Environ. 276 (2020), 119172.
[36] Q. Yang, H. Peng, Q. Zhang, X. Qian, X. Chen, X. Tang, S. Dai, J. Zhao, K. Jiang, Q. Yang, J. Sun, L. Zhang, N. Zhang, H. Gao, Z. Lu, L. Chen, Atomically dispersed high-density Al-N_4 sites in porous carbon for efficient photodriven CO_2 cycloaddition, Adv. Mater. 33 (2021), e2103186.
[37] Q. Yang, C.-C. Yang, C.-H. Lin, H.-L. Jiang, Metal-organic-framework-derived hollow N-doped porous carbon with ultrahigh concentrations of single Zn atoms for efficient carbon dioxide conversion, Angew. Chem. Int. Ed. 58 (2019) 3511–3515.
[38] X. Zhang, H. Liu, P. An, Y. Shi, J. Han, Z. Yang, C. Long, J. Guo, S. Zhao, K. Zhao, H. Yin, L. Zheng, B. Zhang, X. Liu, L. Zhang, G. Li, Z. Tang, Delocalized electron effect on single metal sites in ultrathin conjugated microporous polymer nanosheets for boosting CO_2 cycloaddition, Sci. Adv. 6 (2020) eaaz4824.
[39] J. Sirijaraensre, P. Khongpracha, J. Limtrakul, Mechanistic insights into CO_2 cycloaddition to propylene oxide over a single copper atom incorporated graphene-based materials: a theoretical study, Appl. Surf. Sci. 470 (2019) 755–763.
[40] L. Gong, J. Sun, Y. Liu, G. Yang, Photoinduced synergistic catalysis on Zn single-atom-loaded hierarchical porous carbon for highly efficient CO_2 cycloaddition conversion, J. Mater. Chem. A 9 (2021) 21689–21694.
[41] A.C. Kathalikkattil, D.-W. Kim, J. Tharun, H.-G. Soek, R. Roshan, D.-W. Park, Aqueous-microwave synthesized carboxyl functional molecular ribbon coordination framework catalyst for the synthesis of cyclic carbonates from epoxides and CO_2, Green Chem. 16 (2014) 1607–1616.
[42] J. Song, Z. Zhang, S. Hu, T. Wu, T. Jiang, B. Han, MOF-5/n-Bu_4NBr: an efficient catalyst system for the synthesis of cyclic carbonates from epoxides and CO_2 under mild conditions, Green Chem. 11 (2009) 1031–1036.
[43] Y. Yuan, J. Li, X. Sun, G. Li, Y. Liu, G. Verma, S. Ma, Indium-organic frameworks based on dual secondary building units featuring halogen-decorated channels for highly effective CO_2 fixation, Chem. Mater. 31 (2019) 1084–1091.
[44] P.-Z. Li, X.-J. Wang, J. Liu, J.S. Lim, R. Zou, Y. Zhao, A triazole-containing metal-organic framework as a highly effective and substrate size-dependent catalyst for CO_2 conversion, J. Am. Chem. Soc. 138 (2016) 2142–2145.
[45] W.-Y. Gao, Y. Chen, Y. Niu, K. Williams, L. Cash, P.J. Perez, L. Wojtas, J. Cai, Y.-S. Chen, S. Ma, Crystal engineering of an nbo topology metal-organic framework for chemical fixation of CO_2 under ambient conditions, Angew. Chem. Int. Ed. 53 (2014) 2615–2619.
[46] P. Wu, Y. Li, J.-J. Zheng, N. Hosono, K. Otake, J. Wang, Y. Liu, L. Xia, M. Jiang, S. Sakaki, S. Kitagawa, Carbon dioxide capture and efficient fixation in a dynamic porous coordination polymer, Nat. Commun. 10 (2019) 4362.
[47] N. Wei, Y. Zhang, L. Liu, Z.-B. Han, D.-Q. Yuan, Pentanuclear Yb(III) cluster-based metal-organic frameworks as heterogeneous catalysts for CO_2 conversion, Appl. Catal. B: Environ. 219 (2017) 603–610.
[48] Z. Fang, Z. Deng, X. Wan, Z. Li, X. Ma, S. Hussain, Z. Ye, X. Peng, Keggin-type polyoxometalates molecularly loaded in Zr-ferrocene metal organic framework nanosheets for solar-driven CO_2 cycloaddition, Appl. Catal. B: Environ. 296 (2021), 120329.
[49] Z. Guo, X. Cai, J. Xie, X. Wang, Y. Zhou, J. Wang, Hydroxyl-exchanged nanoporous ionic copolymer toward low-temperature cycloaddition of atmospheric carbon dioxide into carbonates, ACS Appl. Mater. Interfaces 8 (2016) 12812–12821.
[50] Z. Guo, Q. Jiang, Y. Shi, J. Li, X. Yang, W. Hou, Y. Zhou, J. Wang, Tethering dual hydroxyls into mesoporous poly(ionic liquid)s for chemical fixation of CO_2 at ambient conditions: a combined experimental and theoretical study, ACS Catal. 7 (2017) 6770–6780.
[51] G. Chen, Y. Zhang, J. Xu, X. Liu, K. Liu, M. Tong, Z. Long, Imidazolium-based ionic porous hybrid polymers with POSS-derived silanols for efficient heterogeneous catalytic CO_2 conversion under mild conditions, Chem. Eng. J. 381 (2020), 122765.
[52] Y. Tong, B. Zhang, C. Li, L. Xu, Copolymerization of acrylonitrile/1-vinyl-3-ethylimidazolium bromide and rheological, thermal properties of the copolymer, Trans. Tianjin Univ. 25 (2019) 85–90.
[53] G. Férey, M. Latroche, C. Serre, F. Millange, T. Loiseau, A. Percheron-Guégan, Hydrogen adsorption in the nanoporous metal-benzenedicarboxylate M(OH)(O_2C-C_6H_4-CO_2) ($M = Al^{3+}$, Cr^{3+}), MIL-53, Chem. Commun. (2003) 2976–2977.
[54] M. Ding, H.-L. Jiang, Incorporation of imidazolium-based poly(ionic liquid)s into a metal-organic framework for CO_2 capture and conversion, ACS Catal. 8 (2018) 3194–3201.
[55] Y. He, X. Li, W. Cai, H. Lu, J. Ding, H. Li, H. Wan, G. Guan, One-pot multiple-step integration strategy for efficient fixation of CO_2 into chain carbonates by azolide anions poly(ionic liquid)s, ACS Sustain. Chem. Eng. 9 (2021) 7074–7085.
[56] W.-L. Dai, B. Jin, S.-L. Luo, S.-F. Yin, X.-B. Luo, C.-T. Au, Cross-linked polymer grafted with functionalized ionic liquid as reusable and efficient catalyst for the cycloaddition of carbon dioxide to epoxides, J. CO2 Util. 3–4 (2013) 7–13.
[57] P. Puthiaraj, S. Ravi, K. Yu, W.-S. Ahn, CO_2 adsorption and conversion into cyclic carbonates over a porous $ZnBr_2$-grafted N-heterocyclic carbene-based aromatic polymer, Appl. Catal. B: Environ. 251 (2019) 195–205.
[58] J.-I. Yu, H.-J. Choi, M. Selvaraj, D.-W. Park, Catalytic performance of polymer-supported ionic liquids in the cycloaddition of carbon dioxide to allyl glycidyl ether, React. Kinet. Mech. Catal. 102 (2011) 353–365.
[59] M. Liu, B. Liu, S. Zhong, L. Shi, L. Liang, J. Sun, Kinetics and mechanistic insight into efficient fixation of CO_2 to epoxides over N-heterocyclic compound/$ZnBr_2$ catalysts, Ind. Eng. Chem. Res. 54 (2015) 633–640.
[60] Q. Yang, Y. Wang, X. Tang, Q. Zhang, S. Dai, H. Peng, Y. Lin, Z. Tian, Z. Lu, L. Chen, Ligand defect density regulation in metal-organic frameworks by functional group engineering on linkers, Nano Lett. 22 (2022) 838–845.
[61] X. Zhang, X. Zhang, H. Dong, Z. Zhao, S. Zhang, Y. Huang, Carbon capture with ionic liquids: overview and progress, Energy Environ. Sci. 5 (2012) 6668–6681.
[62] F. Castro-Gmez, G. Salassa, A.W. Kleij, C. Bo, A. DFT, study on the mechanism of the cycloaddition reaction of CO_2 to epoxides catalyzed by Zn(salphen) complexes, Chem. Eur. J. 19 (2013) 6289–6298.
[63] F.D. Monica, A. Buonerba, A. Grassi, C. Capacchione, S. Milione, Glycidol: an hydroxyl-containing epoxide playing the double role of substrate and catalyst for CO_2 cycloaddition reactions, ChemSusChem 9 (2016) 3457–3464.
[64] K.J. Laidler, M.C. King, Development of transition-state theory, J. Phys. Chem. 87 (1983) 2657–2664.